Polydisperse Anisotropic Brushes

Victor M. Amoskov and Tatiana M. Birshtein*

Institute of Macromolecular Compounds, Academy of Sciences of Russia, 31,Bolshoj pr., St. Petersburg 199004, Russia

Received December 21, 2000; Revised Manuscript Received April 19, 2001

ABSTRACT: The influence of polydispersity on liquid-crystalline ordering in anisotropic polymer brushes is considered. It is shown that mixing of long and short chains in a brush inhibits LC ordering of long chains; LC ordering is influenced by details of the inner structure of a brush rather than by its global average characteristics. There exists a regime of LC ordering in which the transition point is governed by the length of the short chains and the overall grafting density only, independent of the brush content. After LC ordering of the short chains is finalized, the ordering of long chains may proceed as a second-order phase transition.

1. Introduction

Properties of polymer brushes and brushlike systems have attracted great attention for the past two decades (see refs 1−4 and references therein). This paper continues the study of liquid-crystalline (LC) ordering in planar polymer brushes formed by macromolecules with mesogenic groups in the main chains.[5−15] Bearing in mind orientational anisotropy of segment−segment interactions, we refer to such brushes as to *anisotropic brushes*.

All the previous papers deal with anisotropic brushes formed by monodisperse chains (monodisperse brushes). In this paper we consider anisotropic brushes formed by chains of different contour length (polydisperse brushes) and investigate effects of chain polydispersity on their thermodynamics and conformational properties. As the simplest example of a polydisperse brush, we investigate a bidisperse brush, i.e., a brush formed by chains of two different contour lengths.

The method of theoretical analysis of LC ordering in anisotropic brushes applied here is similar to that of ref 8. In the next section, we take a brief look at this method and introduce its modification for polydisperse brushes. Section 3 gives a review of the relevant results obtained previously for anisotropic monodisperse brushes. New results are presented in sections 4−6. Bidisperse brushes with isotropic interaction were investigated in a number of papers.[16−18] The main results of these papers important for interpreting our new findings are given in section 5.

Before proceeding further, let us stress that the aim of this paper is to investigate general effects of bidispersity (polydispersity) on LC ordering in polymer brushes. Our method of investigation provides numerical solutions of the self-consistent-field theory equations, and we restrict our attention to a qualitative analysis of these solutions.

2. Model and Notations

Following Flory,[19] we construct an equilibrium theory in the self-consistent-field (SCF) approximation and split the free energy functional into two parts—the entropy of noninteracting chains and the energy of short-range interactions—so the dimensionless (in kT units) free energy F of the system is

$$F(\{\rho\},\{U\}) = \int f_{\text{int}}(x)\, \mathrm{d}x \; - \; S[\{U\}] \qquad (1)$$

where $\rho(x)$ is the density of segments in the layer x (x direction is perpendicular to the grafting surfaces, brushes are assumed to be homogeneous in lateral directions; see also section "Conclusion"), $U(x)$ is the SCF potential, $f_{\text{int}}(x)$ is the density of the free energy of short-range interactions, S is the entropy of a system of noninteracting chains under external field U, and braces are introduced to identify the function as a whole as opposed to its value at some layer x.

All the N segments of each chain, grafted with the grafting density σ, are assumed to be mesogenic; i.e., the energy of interaction between segments coming in contact depends on their mutual orientation. For calculating f_{int}, we use a combination of the Flory−Huggins approach (to account for the isotropic part of interaction)[19,20] and the Mayer−Saupe expression for the anisotropic interaction:[21]

$$f_{\text{int}}(x) = (1 - \rho(x)) \ln(1 - \rho(x)) - \chi\rho^2(x) - \frac{\eta}{2}\rho^2(x)s_2{}^2(x) \qquad (2)$$

where χ and η are the parameters of isotropic and anisotropic parts of the segment−segment interaction (energy of interaction divided on kT), and s_2 is the nematic order parameter describing the orientation of segments (with respect to x axis).

The chains are modeled by ideal walks on a simple cubic lattice. The statistical weights (α_t, α_g, α_b) of various local conformations for direct (trans isomer), turn (gauche isomer), and back steps, respectively, are model parameters. The lattice constant is used as a unit length.

Minimization of F leads to a set of equations for calculating the equilibrium density profile $\rho(x)$ and other characteristics in the SCF approximation. To solve the lattice version of these equations, we use the Scheutjens−Fleer numerical method[22] developed for polymer brushes.[4,23−25] The method is based on the self-consistency property of $\rho(x)$ and $U(x)$ which allows one to use an iteration procedure. Choosing the initial approximation for $U(x)$, one can obtain $\rho(x)$, then the next approximation for $U(x)$, and so on.

A necessary refinement for extending this method to anisotropic brushes with orientation-dependent interac-

10.1021/ma002178b CCC: $20.00
Published on Web 06/22/2001

tions involves[8] splitting each of the self-consistent functions $\rho(x)$ and $U(x)$ into sets of three, according to different spatial orientations:

$$\rho \rightarrow (\rho^{\odot}, \rho^{+}, \rho^{\otimes}) \quad \text{and} \quad U \rightarrow (U^{\odot}, U^{+}, U^{\otimes})$$

where the upper index i takes the values of $i = \odot, +, \otimes$ and identifies directions upward, parallel, and downward the grafting plane. A modification of Scheutjens–Fleer algorithm allows one to compute the density components from the SCF potential and vice versa.[8] The segment density and the order parameter are calculated as follows:

$$\rho(x) = \rho^{\odot}(x) + \rho^{+}(x) + \rho^{\otimes}(x)$$

$$s_2(x) = \frac{3\langle \cos^2 \theta(x)\rangle - 1}{2} = \frac{3}{2}\frac{\rho^{\odot}(x) + \rho^{\otimes}(x)}{\rho(x)} - \frac{1}{2}$$

The next step required is extending the method to polydisperse brushes. We treat a polydisperse brush as consisting of K subbrushes ($K = 2$ in the case of bidisperse brushes). We use the term "subbrush" to describe the kth fraction of the brush-forming chains ($k = 1, ..., K$). Chains belonging to one fraction are identical in all characteristics (contour length N_k, statistical weights of conformations $\alpha_{t,k}$, $\alpha_{g,k}$, $\alpha_{b,k}$, etc.). In this paper we take the same statistical weights for all fractions: $\alpha_{t,k} = \alpha_{g,k} = \alpha_{b,k}$ regardless of k. Each subbrush is characterized by its own grafting density σ_k. Since all of them have a common grafting surface, the overall grafting density σ is the sum of σ_k.

It is important that each polymer chains is subject to one and the same self-consistent anisotropic field $U^i(x)$, formed by all the chains in the brush. For a given potential $U^i(x)$, one can compute independently all the partial density profiles $\rho_k^i(x)$ using the algorithm mentioned above[8] (here as before $i = \odot, +, \otimes$ and $k = 1, ..., K$) to find the overall density profile as

$$\rho(x) = \sum_{k,i} \rho_k^i(x) \tag{3}$$

In the case of polydisperse brushes, the iteration procedure starts from some initial approximation for $U^i(x)$. Then, we obtain $\rho_k^i(x)$, $\rho(x)$, then the new $U^i(x)$, etc. The procedure is iterated until the stationary point is reached up to a given tolerance. The final density profile is the solution which minimizes the free energy functional. It should be noted that depending on the starting point of the iteration procedure the minimum found could be global (corresponding to the true equilibrium state) or only local (describing a metastable state).

This method allow us also to investigate a system of two planar brushes separated by distance H and oriented face-to-face. It was noted in ref 11 that this problem may be reduced to that of computing the density profile $\rho(H - x)$ in the external field $U(H - x)$. Using the notion of "subbrushes" allows us to take into account polydispersity of interacting oncoming brushes as well.

3. Key Futures of LC Transition in Anisotropic Monodisperse Brush

To understand better the peculiarities of LC ordering in polydisperse anisotropic brushes, it is reasonable to start with a brief overview of LC transition in monodisperse brushes.[5–15] As long as the energy of anisotropic interaction η is small enough, the density profile of the brush is similar to that at $\eta = 0$. This we call the conventional brush (CB) regime which continues until η reaches a certain critical value. At that point, a small fraction of chains, scaled as $N^{-1/2}$, collapse near the grafting plane, and the brush splits into two layers. The inner layer near the grafting plane has high density and strong orientational order, $\rho \sim 1$ and $s_2 \sim 1$. The outer swollen layer has low density and small degree of order. We refer to this situation as the microsegregated brush (MSB) regime.[8]

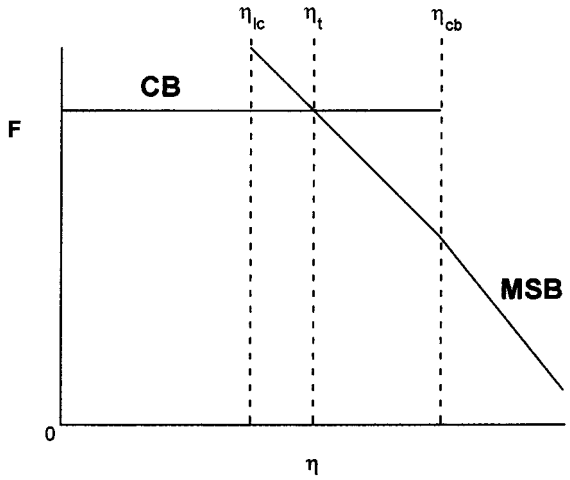

Figure 1. Sketch of the free energy vs the energy of anisotropic interaction in a monodisperse brush, $\sigma < 0.2$.

With the increase in energy η, the inner LC layer is grown at the expense of the outer CB layer until fully LC brush is formed. This we call the LC brush regime.[5] In some cases we use the term "LC brush" as a common term for both MSB and LC regimes, bearing in mind the presence of a LC layer in the brush (although it might be quite small).

In brushes of any finite length N at relatively small grafting densities, $\sigma < 0.2$, the transition from CB to MSB regime with increasing energy η has the following feature. The calculated free energy F (or the chemical potential) turns out to be a two valued function; see Figure 1. It consists of two intersecting branches (CB and MSB/LC), the intersection point at η_t being a first-order phase transition point. The equilibrium CB regime exists at $\eta < \eta_t$; the equilibrium MSB/LC regime exists at $\eta > \eta_t$. The method of computation allows us to study both equilibrium and metastable states. A metastable CB brush exists at $\eta_t < \eta < \eta_{cb}$ (LC brush at $\eta_{lc} < \eta < \eta_t$). The free energy of metastable states is higher than that of the equilibrium state. Metastable CB (or LC) states can be reached in the process of computation starting from the equilibrium states at $\eta = \eta_t$ by successive increase (or decrease) in energy η (hysteresis effect).

The position of the CB–MSB transition point (the value of anisotropic energy η_t), and both end points η_{cb} and η_{lc} defining the bounds of the metastability regions are functions of the chain length N, the grafting density σ, and the solvent quality characterized here in terms of the Flory parameter χ.

The set of values η_t for various values of N, σ, and χ defines a certain dividing surface in the multidimensional diagram of brush states. Correspondingly, the sets of values η_{cb} and η_{lc} define the surfaces where the metastable states disappear.

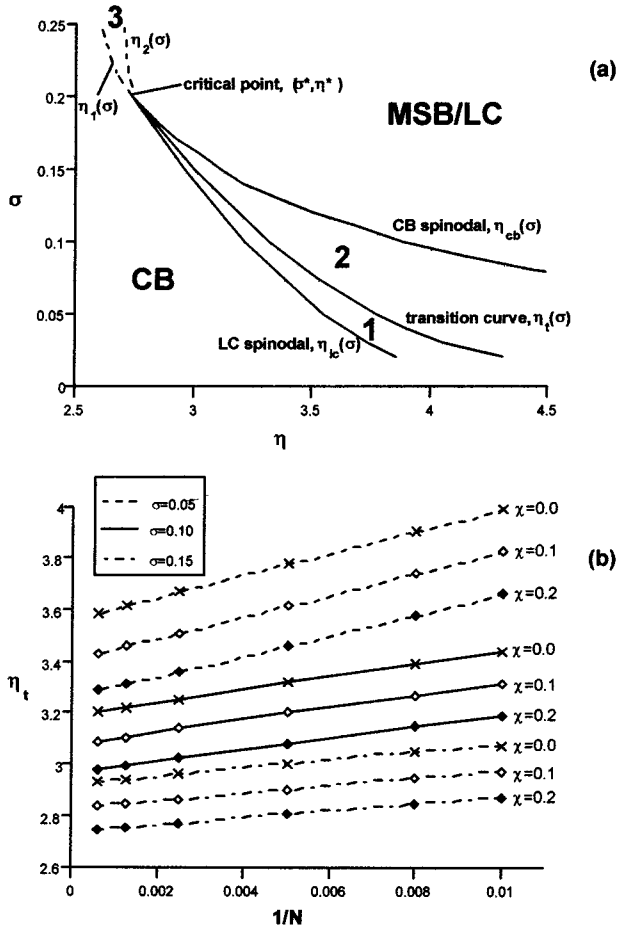

Figure 2. Phase diagrams of an anisotropic brush. (a) Phase diagram in variables (σ,η). Transition curve $\eta_t(\sigma)$ and both spinodals $\eta_{cb}(\sigma)$ and $\eta_{lc}(\sigma)$ are shown by solid lines. The marked areas are: CB, only the conventional brush is possible; LC/MSB, only the microsegregated brush or fully LC brush is possible; 1, CB state is equilibrium and MSB state is metastable; 2, MSB state is equilibrium and CB state is metastable; 3, the regime of overgrafted brush, there is no difference between CB and MSB states (the boundaries of this area $\eta_1(\sigma)$ and $\eta_2(\sigma)$ are shown by dashed lines); $N = 200$, $\chi = 0$. (b) Transition point η_t vs N for a set of values of grafting densities σ and Flory parameters χ (indicated in the graph).

Let us investigate in detail the two-dimensional diagram of states in the (σ,η) coordinates only, the N and χ values being fixed. A typical diagram of states for a brush with $N = 200$ and solvent strength $\chi = 0$ is shown in Figure 2a. It contains a curve $\eta_t(\sigma)$ (the transition curve) and the curves $\eta_{cb}(\sigma)$ and $\eta_{lc}(\sigma)$ (spinodals). This diagram is similar to a well-known liquid−vapor diagram in (P, T^{-1}) variables, with η as T^{-1} and σ as P. In both diagrams the transition curve as well as the two spinodal curves terminate at a critical point, in our case at the point denoted as (η^*,σ^*). CB and MSB/LC regions in this diagram are analogous to vapor and liquid regions in the (P,T^{-1}) diagram, respectively. Regions 1 and 2 between the transition line and the spinodals are regions of coexistence of stable and metastable states: below the transition curve (region 1) CB is stable, MSB is metastable; above the transition line (region 2) the situation is reversed—LC/MSB is stable, CB is metastable. Supercritical (supergrafted) condition is given by $\sigma > \sigma^*$: in region 3 there is no difference between CB and MSB states, and the boundaries $\eta_1(\sigma)$ and $\eta_2(\sigma)$ are not strictly defined.

In this work, we are mostly interested in true equilibrium states; hence, we restrict ourselves to discussing the transition surface $\eta_t(N,\sigma,\chi)$ only. Figure 2b shows the curves $\eta_t(N)$ for a number of values of σ and χ. All the lines in Figure 2b as well as in Figures 1 and 2a are obtained from the numerical solutions of SCF equations. It is interesting to point out that calculation results suggest a linear dependence $\eta_t(N) - \eta_t(\infty) \sim N^{-1}$, which does not agree with analytical asymptotics.[26] For the future discussion, however, only the direction of the effect is important: the value of η_t decreases with the increase in N, χ, or σ.

As an illustration of $\eta_t(N)$ dependence let us consider the possible states of two noninteracted brushes with equal grafting densities $\sigma = 0.1$ and different chain lengths $N_1 = 400$ and $N_2 = 200$. To make the picture more clear, brushes are shown oriented face-to-face; see Figure 3. Figure 4 presents the curves $F(\eta)$ covering all the regimes. Dense layers $\rho \sim 1$ near the grafting surfaces correspond to LC microphases (with high degree of order, $s_2 \sim 1$) in MSB states. The sequence of parts a, b, c of Figure 3 depicts successive equilibrium states as η is increased: the system of two CB brushes (Figure 3a) is stable at $\eta < \eta_t(N_1)$, the system of a long MSB brush and a short CB brush (Figure 3b) is stable at $\eta_t(N_1) < \eta < \eta_t(N_2)$, and the system of two MSB/LC brushes (Figure 3c) is stable at $\eta > \eta_t(N_2)$. Recall that η is the reduced energy parameter, i.e., energy in kT units; hence, an increase in η is equivalent to a decrease in temperature. Points A and B where the slope of the equilibrium free energy $F(\eta)$ (thick solid line in Figure 4) changes discontinuously are the points of the first-order phase transitions in the long and short brush, respectively.

The data in Figures 3 and 4 are in agreement with Figure 2b: the longer brush requires lower energy of anisotropic interaction to achieve partial LC ordering. In other words, the longer brush attains the LC state earlier in the process of increase in η. The state shown in Figure 3d (a long CB brush and a short MSB brush) cannot be obtained as an equilibrium state in a system of noninteracting brushes.

In the next sections, we show that the mixing of long and short chains in a bidisperse brush results in a reversed picture of LC ordering: short chains are the first to form the LC microphase.

Note that all the states shown in Figure 3a−d can exist simultaneously (at one and the same η), most of them being metastable. The free energies of metastable states are shown in Figure 4 by thinner lines. The computational procedure leading to these structures was performed at fixed value of η, namely $\eta_t(N_1) < \eta = 3.3 < \eta_t(N_2)$ and four different starting points. From the technical point of view it was convenient to place separated noninteracting brushes face-to-face as shown in Figure 3, and calculations were done for the system as a whole. It is clear that, under the chosen value of η, only the structure of Figure 3b is at equilibrium. Structures of Figure 3a,c contain one stable and one metastable brush, whereas both brushes of Figure 3d are metastable (Figure 4).

4. Effects of Polydispersity on the LC Transition

We now proceed to a study of LC transition in polydisperse brushes, i.e., brushes formed by a groups of grafted chains with different lengths (groups of

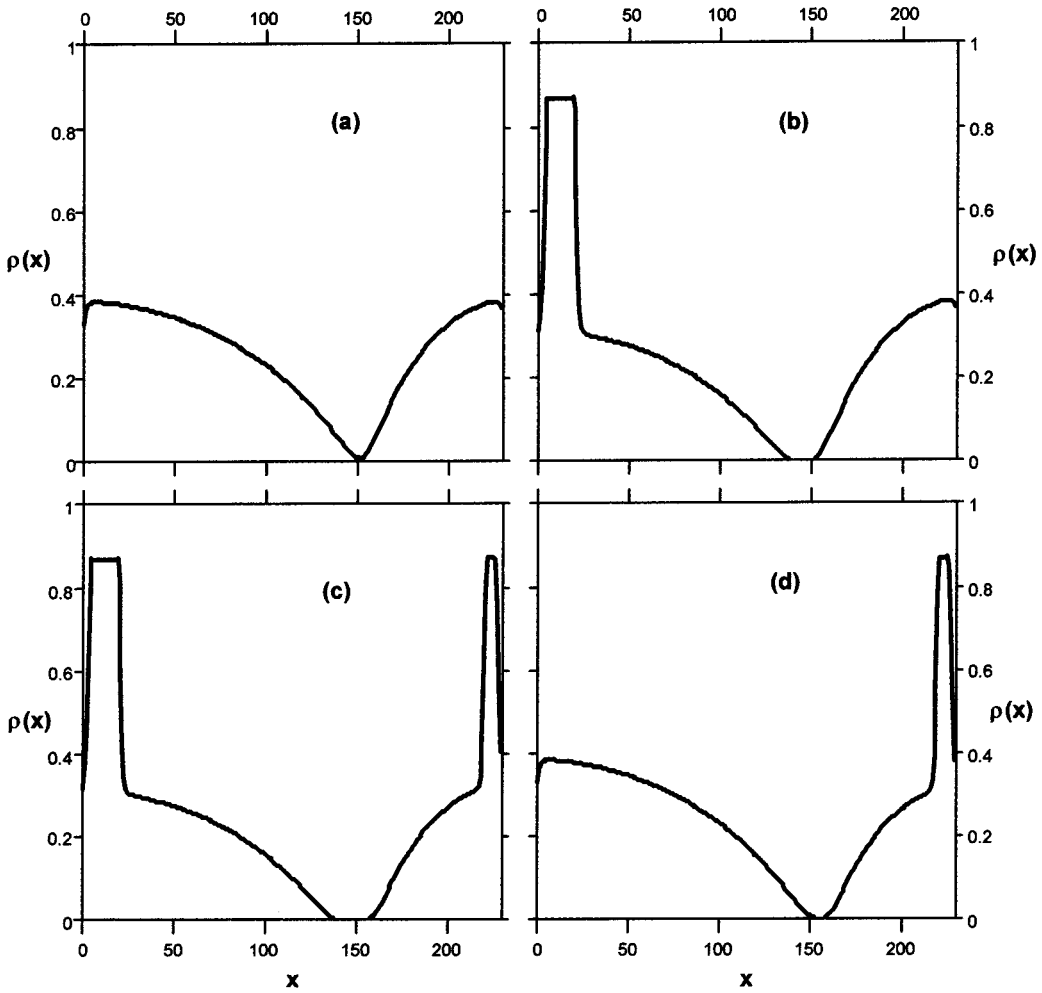

Figure 3. Possible states of a pair of noninteracting anisotropic brushes; $\chi = 0$, $\sigma_1 = \sigma_2 = 0.1$, $N_1 = 400$, $N_2 = 200$, the distance x between grafting surfaces of opposite brushes is larger than the sum of their thicknesses. The sequence of (a)−(c) depicts successive equilibrium states as η increases; the state in (d) is not the equilibrium one (see text for details).

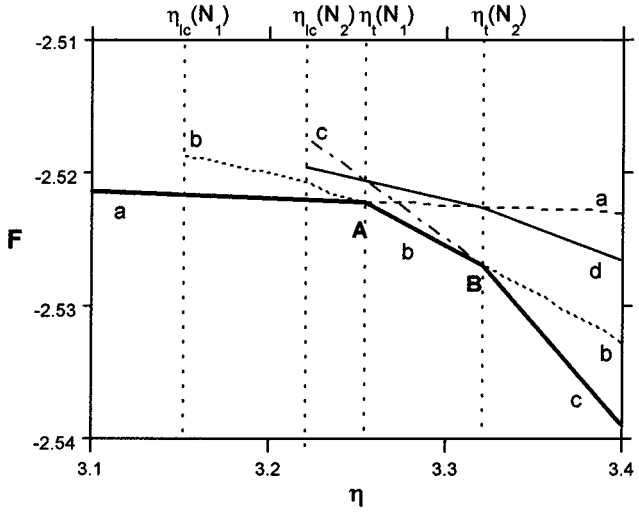

Figure 4. Free energy curves $F(\eta)$ for the four states of a pair of noninteracting anisotropic brushes (the parameters are the same as in Figure 3; letters a−d correspond to the four states in Figure 3).

subbrushes). We restrict ourselves to bidisperse brushes formed by two type of chains with degrees of polymerizations $N_1 = N_{\text{long}}$ and $N_2 = N_{\text{short}} \leq N_1$, grafted with partial densities σ_1 and σ_2.

Investigations performed by the numerical SCF method discussed in section 2 demonstrated that the picture of LC ordering in bidisperse brushes is remarkably rich.

In this section we analyze the position of the LC transition as a function of the brush content. The plots of the free energy F, the average density $\langle\rho\rangle$, and the average orientational order parameter $\langle s_2\rangle$ vs the energy η of anisotropic interaction are displayed in Figure 5 for a bidisperse 50:50 brush ($\sigma_1 = \sigma_2 = \sigma/2$). The overall picture agrees completely with our earlier results for monodisperse brushes (see Figures 1 and 2 and also the data of ref 8). It is clear that a bidisperse brush undergoes a pronounced first-order phase transition, provided the overall grafting density is not too large $\sigma = \sigma_1 + \sigma_2 \leq 0.2$. Note that this restriction follows from our unpresented computation and is similar to that investigated for monodisperse brushes (see refs 8 and 13 for details).

Let us now investigate the position of the transition point η_t as a function of the brush composition. Results of numerous calculations are summarized in Figure 6, which depicts one of the key findings of this paper.

Figure 6 presents the dependence of η_t on the fraction of short chains σ_2/σ in a brush at fixed overall grafting density $\sigma = \sigma_1 + \sigma_2$. The data of Figure 6 are plotted for several values of the long chain length N_1 at a fixed short chain length $N_2 = 200$.

The extreme left (right) points in Figure 6 correspond to monodisperse brushes consisting of only long (short) chains. The change in the brush composition from left

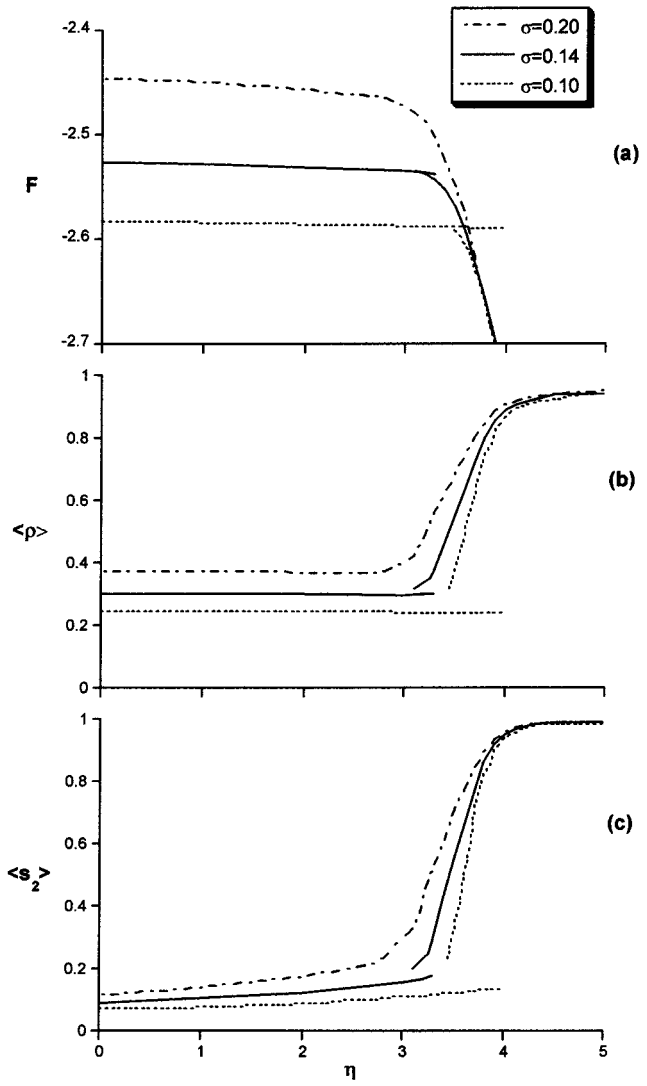

Figure 5. Free energy (a), average segment density (b), and average orientational order parameter (c) vs the energy of anisotropic interaction for a set of grafting densities σ (indicated in the figure). $N_1 = 400$, $N_2 = 200$, $\sigma_1 = \sigma_2 = \sigma/2$, $\chi = 0$.

to right in Figure 6 may be imagined as a result of trimming some of the long chains; the change in composition from right to left corresponds to lengthening some of the short chains. Hence, the total amount grafted, $\sigma_1 N_1 + \sigma_2 N_2$, increases from right to left.

Using the generally accepted idea about regimes of behavior in polymer systems, it may be safely suggested that the curves in Figure 6 point out to the existence of two different regimes of the LC transition in a bidisperse brush. A regime of independence of the η_t on the fraction content σ_1 and σ_2 at fixed $\sigma = \sigma_1 + \sigma_2$ found at the right side of all the curves in Figure 6 (the only exception being the curve for $N_1 = 210$, i.e., at $N_1 \approx N_2$). In other words, in this regime the brush does not "feel" the lengthening of some short chains, and the position of the LC transition remains at the point η_t for a monodisperse short brush (this is the point of $\sigma_1 = 0$). Let us call this regime the short chain transition (SCT) regime. The fact that SCT regime exists is not so surprising by itself; however, its extent is rather surprising. For example, at $N_1 = 800$, it continues down to just ~30% of short chain ($N_2 = 200$) fraction. It is easy to see that in this case about 90% of segments in the brush belong to long chains.

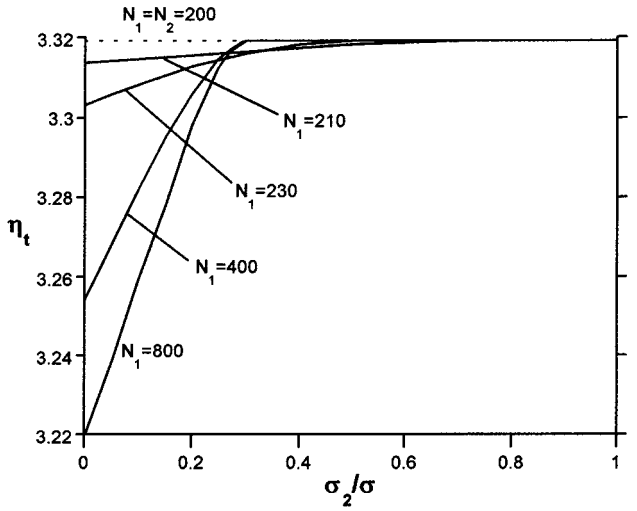

Figure 6. Position of the transition point η_t vs the partial fraction of short subbrush σ_2/σ for a set of chain lengths N_1 of the long subbrush (indicated in the figure). $N_2 = 200$, $\sigma = 0.1$, $\chi = 0$.

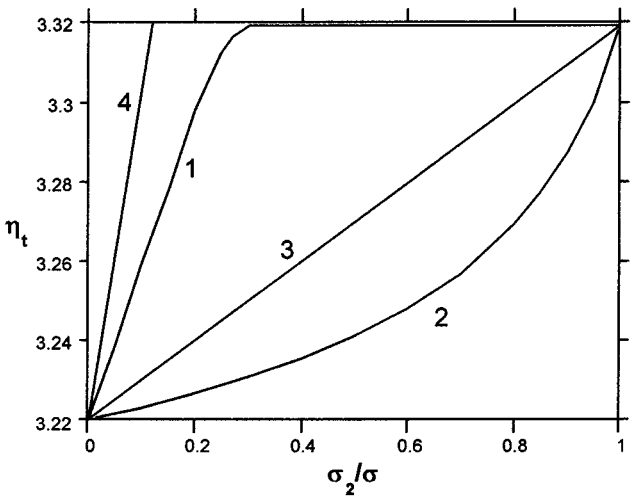

Figure 7. Position of the transition point η_t vs the partial fraction of short subbrush σ_2/σ for chain lengths $N_1 = 800$ and $N_2 = 200$: 1, the same as curve $N_1 = 800$ in Figure 6; 2−4, curves for different monodisperse models of bidisperse brush (see text).

The second regime will be symbolically called as the mixed transition (MT) regime. It is illustrated by the left side of Figure 6. In this case, the transition point η_t depends on all the parameters: $\sigma_{1,2}$ and $N_{1,2}$. The left extreme point corresponds to monodisperse brush consisting of long chains. The longer are the brush chains the lower is the value of energy η at this point; see Figure 2b.

The curves $\eta_t = f(\sigma_2/\sigma)$ for different N_1 intersect each other. This results from the position of crossover between regimes SCT and MT on each curve and from the dependence of this position on N_1. As seen in Figure 6, the larger is difference between N_1 and N_2, the more extent is the SCT regime, and the smaller is the MT region. On the contrary, the MT regime is extended if N_1 and N_2 values are close to each other. For the case $N_1 = 210$, for example, the MT regime expands over the whole range $0 \le \sigma_2/\sigma \le 1$ (Figure 6).

It should be finally noted that the curves presented in Figure 6 are due to mixing polydisperse (bidisperse) chains in the same brush. Figure 7 illustrates this

conclusion. Curve 1 in Figure 7 is a copy of the curve $N_1 = 800$ in Figure 6. Curve 2 in Figure 7 is calculated for a monodisperse brush with the chain length N^* equal to average chain length of the bidisperse brush

$$N^* = \langle N \rangle = \frac{\sigma_1}{\sigma} N_1 + \frac{\sigma_2}{\sigma} N_2$$

Curve 3 is computed for a monodisperse brush ($N = N^{**}$) under suggestion:

$$\frac{1}{N^{**}} = \left\langle \frac{1}{N} \right\rangle = \frac{\sigma_1}{\sigma} \frac{1}{N_1} + \frac{\sigma_2}{\sigma} \frac{1}{N_2}$$

According to Figure 2b, the dependence $\eta_t(N^{**})$ is linear.

Curve 4 is obtained for a monodisperse brush composed of long chains $N_1 = 800$ grafted with grafting density σ_1; i.e., it is supposed that, as we move from left to right, the long chains are removed rather than replaced by the short chains as it happens for curve 1.

Comparing curve 1 to curves 2 and 3, it is clear that η_t value computed for bidisperse brushes is greater than values obtained for simple models. Bidispersity inhibits LC ordering in a brush: simple estimates for equivalent monodisperse brushes lead to smaller values of η_t.

Figure 7 also shows that the dependence $\eta_t(\sigma_2)$ in the MT regime is similar to that for a brush formed by long chains only (i.e., $N_2 = 0$), but the slope of the latter curve is greater than the slope of curve 1.

It is clear that the dependence obtained is closely related to the bidispersity of chains, so it is necessary to analyze in detail the structure of bidisperse brushes at the transition point.

5. Structure of Bidisperse Brush near Phase Transition

We start with a brief analysis of two more simple structures: (1) a monodisperse brush at the point of the LC transition[8] and (2) a bidisperse brush formed by nonmesogenic chains ($\eta = 0$) in a good solvent.[16−18] We will show that the prominent feature of the LC transition in bidisperse brushes has its origin in the peculiarities of these structures.

The structure of a monodisperse brush at the LC transition point is shown in Figure 3 in section 3 and also in Figure 9a of the present section (curve $N_1 = N_2 = 200$). One of two brushes in Figure 3b,d and both brushes in Figure 3c exemplify microphase segregated brushes (MSB): they combine a dense ordered LC inner layer and a swollen CB outer layer. This structure emerges from the CB structure in a discontinuous way at the phase transition point $\eta = \eta_t$. With further increase in η, the inner ordered layer grows at the expense of the outer swollen layer.

For interpreting the results of this paper, it is important to know that chains in the MSB structure are split into two groups: the chains of first group (inner chains) are densely packed in the inner layer; the rest of the chains (transit chains) pass through the inner layer and are still swollen at the brush periphery. Such an interpretation is based on the two-humped free ends distribution function $g(x)$ (see ref 8 and the curve for $N_1 = N_2 = 200$ in Figure 9b). At the transition point η_t, the LC layer is formed by a small fraction (scaled as $N^{-1/2}$) of chains.[8]

It is important also that all chains are strongly oriented inside LC layer. This is true for parts of transit chains as much as for all inner chains; both partial order parameters being equal to each other are near unity.[8]

Figure 8 shows density profiles (Figure 8a,c,e) and free ends distributions (Figure 8b,d,f) for the other system serving as a base of comparison: a conventional bidisperse brush consisting of two subbrushes. Partial grafting densities in Figure 8 are equal: $\sigma_1 = \sigma_2 = 0.05$, the short chain length is fixed at $N_2 = 200$, and data are presented for several lengths of long chains N_1 (all the curves in Figure 8 are marked by the value of N_1). The overall characteristics are shown in Figure 8a,b, the partial data for the short subbrush are shown in Figure 8c,d, and the partial data for the long subbrush are shown in Figure 8e,f. All the curves for $N_1 = 200$ in Figure 8 correspond to a monodisperse short brush: $N_1 = N_2 = 200$.

It is clear from Figure 8 that the total brush consists of two layers under the condition of sufficiently strong difference between the chain lengths (curves $N_1 \geq 300$). The inner layer is more dense, and the outer layer is swollen. This difference in density is connected to the fact that the inner layer is composed of both chain types; i.e., its density is defined by the total grafting density $\sigma = \sigma_1 + \sigma_2$. The short chains are completely confined to the inner layer. The distribution of short chains in this layer is more or less close to that in a monodisperse brush, composed of only the short chains with the partial grafting density σ_2 (see Figure 8c). The thickness of the inner layer is defined by the length of short chains and their fraction.

The variation of the long chain length does not influence the inner layer provided the difference between the chain lengths is sufficiently strong, since all the long chains pass through the inner layer. So the outer layer is formed only by long chains grafted with grafting density σ_1, which is smaller than the total grafting density, $\sigma_1 < \sigma$.

The free ends of all the long chains are dispersed in the outer layer (Figure 8c), and therefore the free ends of the two group of chains (short and long) are segregated. This is clearly demonstrated by bimodal shape of the free ends distribution (Figure 8b).

The degree of overlapping of the free ends of the two group of chains depends on the difference between N_1 and N_2. Previous discussion refers to the case of a large difference between these values. In the case of relatively small difference $(N_1 - N_2)/N_1$ one can see a more or less strong overlapping (curves $N_1 = 210$ and 230 in Figure 8f; the division of chains in two group is purely arbitrary in the limiting case $N_1 = 200$).

Figure 8 presents the data for the "symmetrical" case: $\sigma_1 = \sigma_2 = \sigma/2$. Here, the numbers of grafted chains are in the proportion as 50:50; the number of segments in the two types of chains is in the ratio N_1:N_2.

The general regularities seen in Figure 8 are typical for a wide range of compositions (in terms of the relative partial grafting densities σ_1/σ and σ_2/σ).

Let us now zoom in on the structure of anisotropic bidisperse brush at the point of phase transition $\eta = \eta_t$. Figure 9 presents the data obtained for the "symmetrical" case $\sigma_1 = \sigma_2 = \sigma/2$. All the parameters (except for the value of η) are equal to that in Figure 8. Values of η_t for each N_1 are shown in Figure 6 at $\sigma_2/\sigma = 0.5$. As follows from Figure 6, the change in the long-chain length N_1 in the symmetrical case allows one to investigate both the SCT regime ($N_1 \gg N_2$) and the MT regime ($N_1 \simeq N_2$).

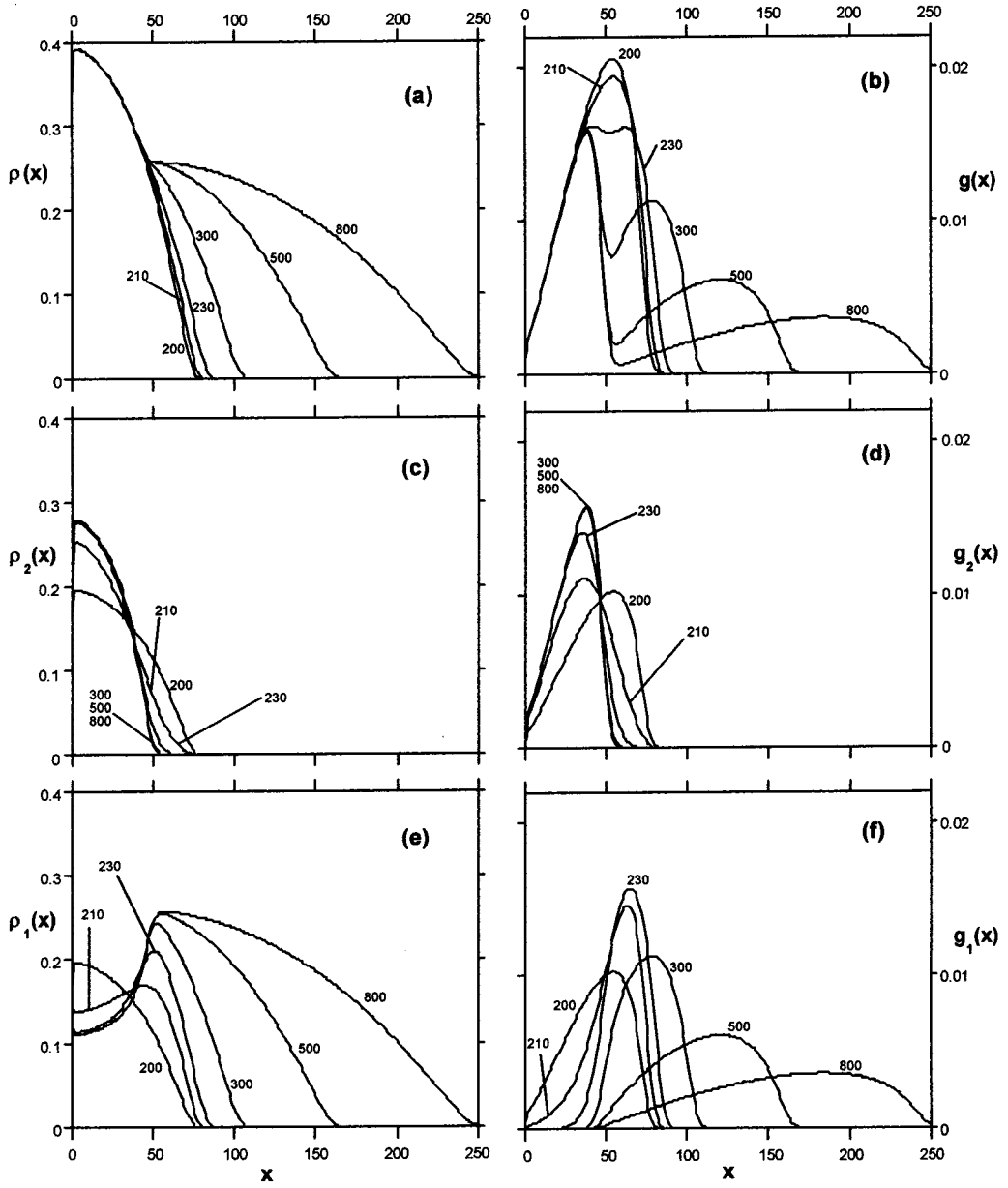

Figure 8. Segment densities (a, c, e) and the free ends distributions (b, d, f) for an isotropic ($\eta = 0$) brush in a good solvent ($\chi = 0$) composed of chains of two lengths: N_1 (indicated at the curves) and $N_2 = 200$. $\sigma_1 = \sigma_2 = 0.05$: (a, b) the overall distributions; (c, d) the short chains distributions; (e, f) the long chain distributions.

Figures 6, 8, and 9 demonstrate that the preexistence of a two-layered structure in the brush at $\eta = 0$ is a necessary condition for the SCT mechanism of the LC transition. In this case, practically only short chains residing in the inner layer take part in forming the new LC phase. Moreover, only a part of short chains is sufficient for producing the LC microphase at the transition point η_t (Figure 9 at $N_1 \geq 300$). The rest of the short chains and all of the long chains continue to be swollen once they pass through an inner LC layer. As a result, the brush appears to be subdivided into three layers: the inner LC layer, a middle layer without strong LC order formed by chains of both types, and an outer swollen disordered layer formed by long chains only. Note that the collapsed LC layer contains also small portions of long transit chains. These portions are strongly oriented as well as all other chains inside LC layer. The degree of orientation is related to overall density inside LC layer rather than to partial densities. According to the unshown results, the partial order parameters inside LC layer are equal to each other, despite the great difference in partial densities (Figure 9c,e). The free ends distribution is three-humped; its three maxima belong to (1) the collapsed part of short chains in the LC layer; (2) the rest of short chains in the swollen medium layer, and (3) the long chains in the outer layer.

Long chains play the role of an unchanging environment, so the length of long chains does not influence neither the position of the transition point η_t nor the thickness of the collapsed domain. This fact explain the occurrence of the SCT regime.

This regime is realized only if the free ends of the two types of chains do not overlap in the starting disordered brush (at $\eta = 0$). This is not the case for a symmetrical brush at $N_1 < 300$ which cannot be divided into two independent layers due to a considerable overlapping of the free ends of short and long chains. This overlapping also takes place at the transition point η_t. Not only short but also long chains participate in formation of

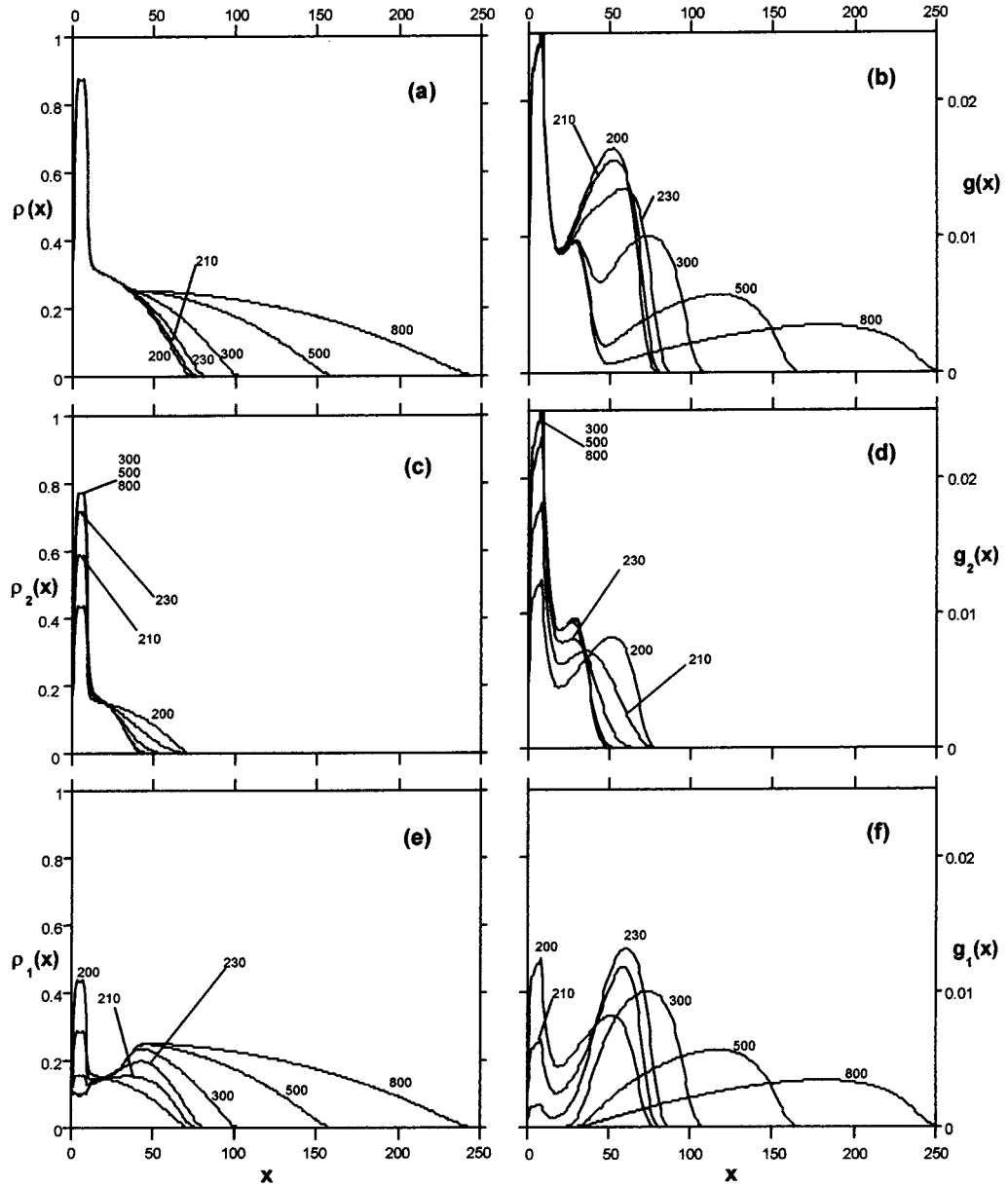

Figure 9. Same as Figure 8 at the phase transition point $\eta = \eta_t$.

the collapsed LC layer. The distribution of free ends of both type of chains becomes two-humped, the first maximum corresponding to chains in the collapsed LC layer and the second to chains in the swollen sublayer (Figure 9, $N_1 = 210$ and 230). As a result, the position of the LC transition η_t depends on length N_1 as well as on N_2. Results for monodisperse brushes (section 3) show that the η_t value decreases with increase in N; in our case η_t also decreases with increase in N_1 (at fixed value of N_2). This picture gives an account of the MT regime in the LC transition.

Note that despite the difference in the distribution of short and long chains in the SCT and the MT regimes, part of the total density profile does not depend on N_1 and coincides with the profile of a monodisperse brush grafted with density σ (Figure 9a, $\rho(x)$ at $x < 40$).

Up until now we analyzed the structure of a 50:50 brush at $\eta = \eta_t$. Here, the LC transition follows SCT or MT mechanism depending on whether the difference between N_1 and N_2 is strong or weak. As follows from Figure 6, the MT regime also takes place for largely different N_1 and N_2, if the fraction of short chains is relatively small. Note that a disordered ($\eta = 0$) bidisperse brush in this case consists of two layers in the same way as a 50:50 brush (Figure 8). Nevertheless, the thickness of the inner layer (similar to one in Figure 8) is too small by itself to produce the LC layer, so long chains also take part in the LC collapse (see Figure 10). The free ends of long chains are divided into two groups, inside and outside the LC layer. Hence, the two-layered structure of a bidisperse unordered brush appears to be a necessary, but not a sufficient, condition for the SCT regime of LC transition.

Let us now return to the SCT regime. In this regime the ordering of a bidisperse brush with increase in η starts with the short chains (Figure 9). It is the opposite to the order in which LC transitions proceed in noninteracting brushes as discussed in section 3: for equal grafting densities, the LC ordering in a "long" brush starts earlier than in a "short" brush.

Mixing chains of different lengths in the same brush preserves the structure of the inner layer and leads to a decrease in grafting and volume densities of the outer layer composed of long chains. Weaker crowding of long

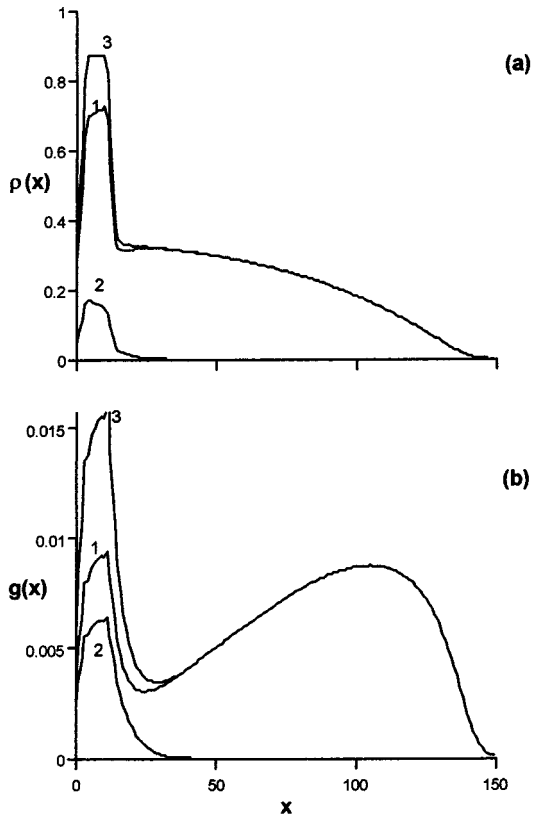

Figure 10. Segment density profiles (a) and the free ends distribution (b) at the phase transition point ($\eta = \eta_t$) for the case of a very small fraction of short chains: 1, the long chains; 2, the short chains; 3, the overall distributions. $N_1 = 800$, $N_2 = 200$, $\sigma_1 = 0.09$, $\sigma_2 = 0.01$, $\chi = 0$.

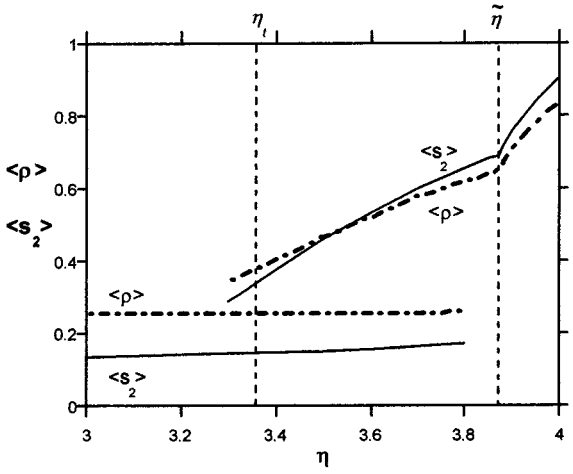

Figure 11. Average segment density and average order parameter vs the energy of anisotropic interaction η for the case of a very high fraction of short chains in the brush. $N_1 = 800$, $N_2 = 200$, $\sigma_1 = 0.01$, $\sigma_2 = 0.09$, $\chi = 0$.

chains in the outer layer is the reason that mixing of chains of different lengths in a disordered brush is thermodynamically favorable (see also refs 17 and 18). This stabilization of the disordered state inhibits LC ordering of long chains. On the other hand, the free energy of the short chains does not get the same benefit and is the same as in a monodisperse brush with the same total grafting density. This is the reason that the long chains in a bidisperse brush remain to be swollen when the short chains have already collapsed into the LC microphase. Replacing part of the long chains by short ones leads to an additional difficulty in long-chain LC ordering.

6. LC Ordering at $\eta > \eta_t$

Until now, we have discussed the emergence of a MSB structure from a CB structure at the transition point η_t. Let us follow this process further as the energy η is increased.

The course of LC ordering in the MT regime (Figure 10 and curves $N_1 = 210$ in Figure 9) is more or less trivial. The LC layer that appeared at $\eta = \eta_t$ was partly formed by long chains, so an increase in η leads to increasing the long chain fraction in the LC layer until a fully LC state is formed.

The case of the SCT regime of ordering is not so simple. Figure 11 displays the average characteristics of a bidisperse brush vs the anisotropic energy η for a case when the number of segments in short chains (about 70%) is greater than that in long chains (about 30%). It is clear that, initially, a first-order phase transition takes place as demonstrated by a discontinuous change in the density and orientational order (see also Figure 5). With increasing η, the curves demonstrate an additional pecularity. At some value of $\tilde{\eta} > \eta_t$, the slope of both curves in Figure 11 changes abruptly. (The same effect is also seen in Figure 5b,c, but it is less pronounced due to a relatively small fraction of short chain segments in the brush.) This means that there appears to be an additional second transition.

Analysis shows that when η approaches the value $\tilde{\eta}$ from below, the LC ordering of short chains is practically completed. Long chains continue to be swollen. The break in the slope in Figure 11 at $\eta = \tilde{\eta}$ corresponds to the beginning of LC ordering of long chains. The presence of a LC layer of short chains leads to the fact that collapse of long chains into the LC phase starts as continuous transition. One might think that this transition could be a phase transition of second (or higher) order.

Figure 12 show the overall and the partial density profiles and free ends distributions in a bidisperse brush undergoing LC ordering in the SCT regime for successive stages of the LC ordering. Figure 12a,b demonstrates the first stage of ordering at $\eta = \eta_t$. We discussed this structure in the previous section.

Figure 12c,d is obtained for η slightly larger than $\tilde{\eta}$—the second transition point. It is seen that some of the long chains participate now in forming the LC layer. Moreover, long chains in structure described by Figure 12c appear to be divided into two groups: some are collapsed inside the LC phase, and the others pass through this phase to the swollen periphery of the brush (similar to what happened to short chains in Figure 12a). The distribution of long-chain free ends (Figure 12d) is two-humped. At this stage, one can see some peculiarity of the short-chain distribution. With the inclusion of long chains in the LC phase the thickness of this phase increases. This provides an opportunity for short chains to ease their contraction inside the LC layer, which they do not hesitate to take. This effect is especially pronounced in Figure 12e, demonstrating the final stage of LC ordering. The density profile of short chains is extended over the whole thickness of the LC brush. The shape of this profile is similar to a familiar parabolic form in conventional brush. Note that, in

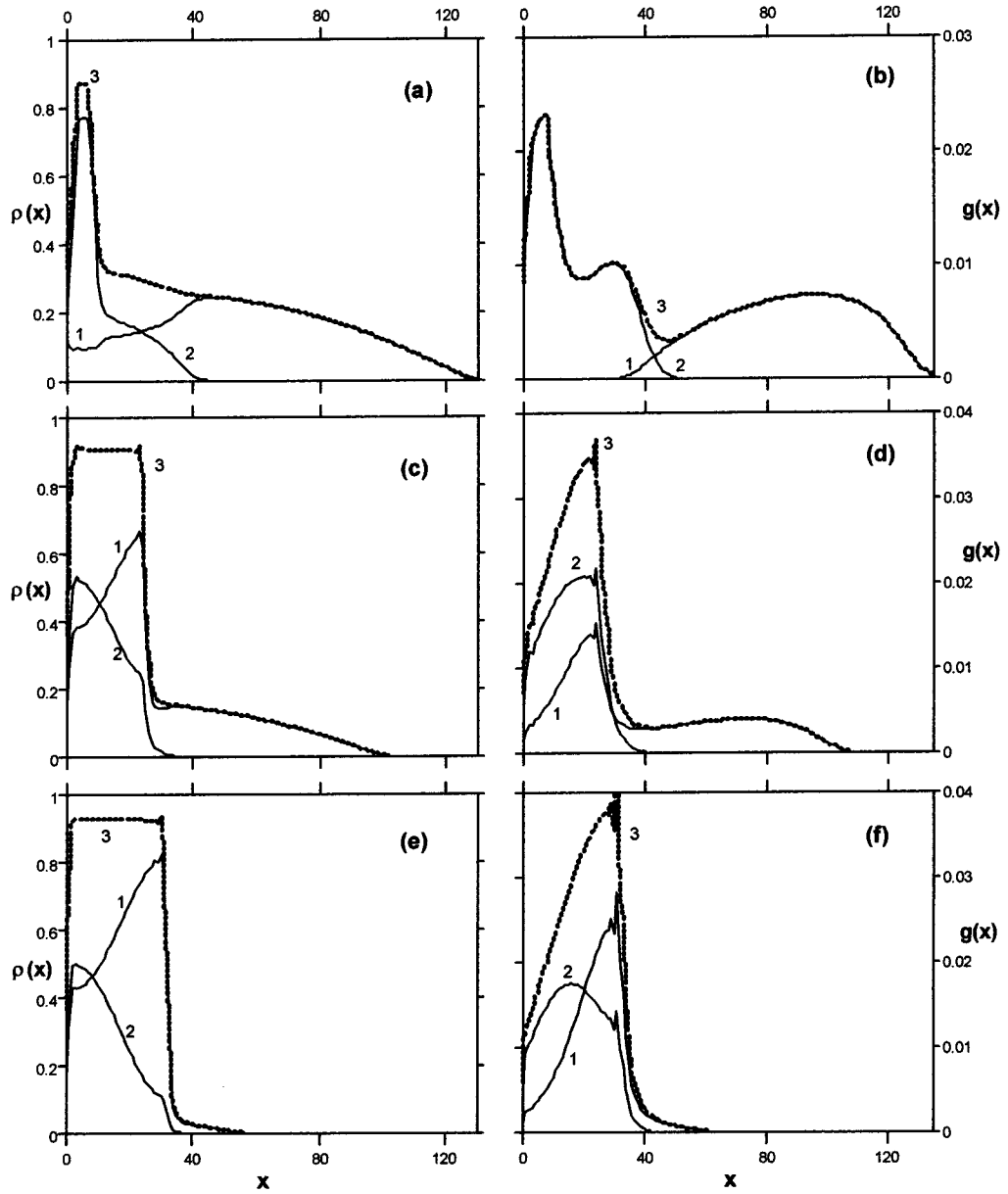

Figure 12. Evolution of partial and total density profiles (a, c, e) and free ends distributions (b, d, f) in a polydisperse anisotropic brush: (a,b) $\eta = \eta_t = 3.3$, (c,d) $\eta = 3.7$, (e,f) $\eta = 4$. 1, long subbrush $N_1 = 400$; 2, short subbrush $N_2 = 200$; 3, total brush; $\sigma_{1,2} = 0.05$, $\chi = 0$.

contrast to conventional brushes, the overall profile of the a LC brush is boxlike.

Finally, Figure 13 shows the manifestation of all these effects in bidisperse brush on the η dependences of its average partial characteristics. For comparison, the similar dependences for monodisperse brush are also shown. One can see that mixing of short and long chains inhibits not only ordering of long chains but also the overall ordering. In contrast, $\langle s_2 \rangle$ vs η curve for short subchains becomes steeper. We also call attention on the nonmonotonic dependence of $\langle \rho_2 \rangle$ on η for short subbrush which results from the reconstruction of intrinsic brush structure at successive stages of LC ordering (Figure 12). This nonmonotonic dependence of partial density of short chains has no effects on their partial order parameter, which is monotonically increased function of η. It is connected with the fact, many times mentioned in this paper, that partial order parameters inside LC layer are related to the total density rather than to its partial values.

7. Conclusions

This paper deals with the scenarios of LC ordering in bidisperse polymer brushes. It is shown that:

1. Mixing of long and short chains in a brush inhibits LC ordering of long chains.

2. LC ordering is influenced by details of the inner structure of a brush rather than by its global average characteristics.

3. There exists a regime of LC ordering (SCT regime) in which the transition point η_t is governed by the length of short chains and the overall grafting density only, independent of the brush content. The free ends distribution in the SCT regime is three-humped: its three maxima belong to the collapsed part of short chains in the LC layer, the rest of short chains in the swollen medium layer, and the long chains in the outer layer.

4. After LC ordering of short chains is finalized, the ordering of long chains may proceed as a second-order phase transition.

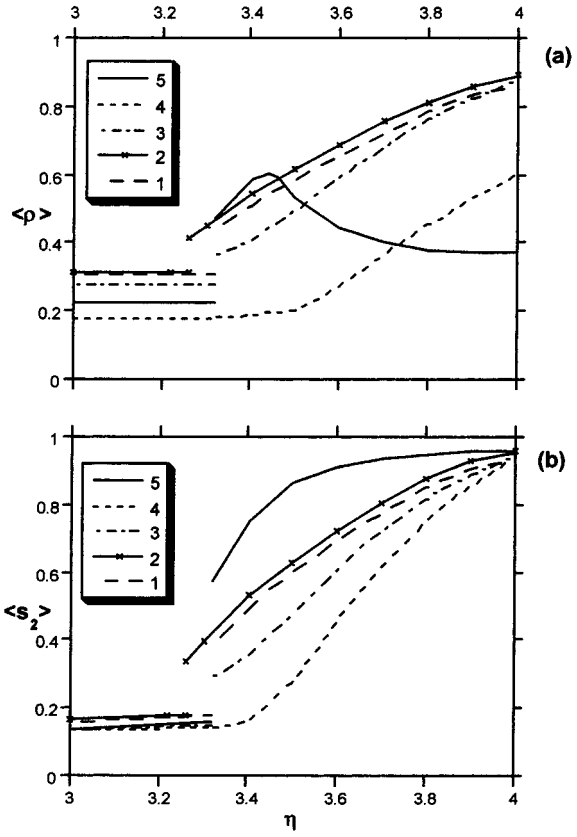

Figure 13. Average segment density (a) and order parameter (b) vs the energy of anisotropic interaction η: 1, monodisperse short brush ($N = 200$); 2, monodisperse long brush ($N = 400$); 3, bidisperse brush ($N_1 = 400$, $N_2 = 200$, $\sigma_{1,2} = \sigma/2$); 4, long subbrush ($N_1 = 400$, $\sigma_1 = \sigma/2$); 5, short subbrush ($N_2 = 200$, $\sigma_2 = \sigma/2$); $\sigma = 0.1$, $\chi = 0$, the metastable states are omitted.

Note also that in this work the qualitative interpretation of results is given only. The quantitative analysis will be presented in the future.[26]

Two remarks in conclusion. The results of this paper are obtained by assuming lateral homogeneity of a brush. In the case of attractive interaction between polymeric segments this assumption is not universally correct. In particular, for a brush in a poor solvent the alternative structure may be conceived. This is a set of micelle-like agregates with core enriched by collapsed polymer and "legs" connecting the core to the grafting surface.[27−30]

Hence, this struture is microsegregated in lateral dimension. It is not possible to a priori exclude such type of structure in the case of LC brushes, especially in bidisperse systems. According to the comment of one of the referees, "one could argue that the long chain could protrude through the LC sublayer of short chains and at the brush periphery form a laterally inhomogeneous layer of clustered chains". However, according to scaling estimation for a brush in a poor solvent,[27−30] the homogeneous collapsed layer is more stable than the set of the separate collapsed clusters provided the condition $N > \sigma^{-2}$ takes place. It seems reasonable to suppose the same situation for the collapsed LC state, even in reference to long chains in the bidisperse brush. If so, the condition $N_2 > \sigma^{-2}$ (as well as $N_1 > \sigma^{-2}$) provides the lateral homogeneity of our system at all stages of ordering.

Acknowledgment. The authors express their gratitude to L. I. Klushin for helpful discussions. We acknowledge the Russian Foundation for Basic Research (Grant 99-03-33319) and INTAS (Grant 99-01852) for financial support.

References and Notes

(1) Milner, S. T. *Science* **1991**, *251*, 905.
(2) Halperin, A.; Tirrel, M.; Lodge, T. P. *Adv. Polym. Sci.* **1992**, *100*, 31.
(3) Birshtein, T. M.; Amoskov, V. M. *J. Polym. Sci., Ser. C* **2000**, *42*, 2286.
(4) Fleer, G. J.; Cohen-Stuart, M. A.; Scheutjens, J. M. H. M.; Cosgrove, T. *Polymer at Interfaces*; Chapman and Hall: London, 1993.
(5) Pickett, G. T.; Witten, T. A. *Macromolecules* **1992**, *25*, 4569.
(6) Kolegov, B. I. Ph.D. Thesis, Leningrad, 1983.
(7) Wijmans, C. M.; Leermakers, F. A. M.; Fleer, G. J. *J. Chem. Phys.* **1994**, *101*, 8214.
(8) Amoskov, V. M.; Birshtein, T. M.; Pryamitsyn, V. A. *Macromolecules* **1996**, *29*, 7240.
(9) Birshtein, T. M.; Mercurieva, A. A.; Pryamitsyn, V. A.; Polotsky, A. A. *Macromol. Theory Simul.* **1996**, *5*, 215.
(10) Birshtein, T. M.; Amoskov, V. M.; Mercurieva, A. A.; Pryamitsyn, V. A. *Macromol. Symp.* **1997**, *113*, 151.
(11) Amoskov, V. M.; Birshtein, T. M.; Pryamitsyn, V. A. *Macromolecules* **1998**, *31*, 3720.
(12) Birshtein, T. M.; Mercurieva, A. A.; Klushin, L. I.; Polotsky, A. A. *Comput. Theor. Polym. Sci.* **1998**, *8*, 179.
(13) Klushin, L. I.; Birshtein, T. M.; Mercurieva, A. A. *Macromol. Theory Simul.* **1998**, *7*, N5, 483.
(14) Birshtein, T. M.; Amoskov, V. A. *Comput. Theor. Polym. Sci.* **2000**, *10*, 159.
(15) Amoskov, V. M.; Birshtein, T. M. *J. Polym. Sci., Ser. A* **2000**, *42*, 392.
(16) Milner, S. T. *Europhys. Lett.* **1988**, *7*, 695. Milner, S. T.; Witten, T. A.; Cates, M. *Macromolecules* **1989**, *22*, 853.
(17) Birshtein, T. M.; Lyatskaya, Yu. V.; Zhulina, E. B. *Polymer* **1990**, *31*, 2185.
(18) Birshtein, T. M.; Lyatskaya, Yu. V.; Zhulina, E. B. *J. Polym. Sci., Ser. A* **1990**, *32*, 1704.
(19) Flory, P. J. *Principles of Polymer Chemistry*; Cornell University Press: Ithaca, NY, 1953.
(20) de Gennes, P. G. *Scaling Concepts in Polymer Physics*; Cornell University Press: Ithaca, NY, 1979.
(21) Maier, W.; Saupe, A. *Z. Naturforsch. A* **1959**, *14*, 882.
(22) Scheutjens, J. M.; Fleer, G. J *J. Phys. Chem* **1979**, *83*, 1619.
(23) Cosgrove, T.; Heath, T.; van Lent, B.; Leermakers, F.; Scheutjens, J. M. *Macromolecules* **1987**, *20*, 1692.
(24) Skvortsov, A. M.; Pavlushkov, I. V.; Gorbunov, A. A. *Polym. Sci.* **1988**, *30*, 487.
(25) Skvortsov, A. M.; Gorbunov, A. A.; Pavlushkov, I. V.; Zhulina, E. B.; Borisov, O. V.; Pryamitsyn, V. A. *Polym. Sci.* **1988**, *30*, 1706.
(26) Klushin, L. I.; Birshtein, T. M.; Amoskov, V. M. *Macromolecules*, in press.
(27) Klushin, L. I., preprint, 1992.
(28) Williams, D. R. M. *J. Phys. II* **1993**, *28*, 1313.
(29) Zhulina, E. B.; Birshtein, T. M.; Pryamitsyn, V. A.; Klushin, L. I. *Macromolecules* **1995**, *28*, 8612.
(30) Lai, P. Y.; Binder, K. *J. Chem. Phys.* **1992**, *97*, 586.

MA002178B